Evaluation of 3D Breast Surface Reconstruction Accuracy Using Non-contact Scanner Images: A Phantom Study

Cuiping Zhang[1,2], Predrag R. Bakic[1], Shugao Xia[2], Fengshan Liu[2], and Andrew D.A. Maidment[1,2]

[1] Department of Radiology, University of Pennsylvania, 3400 Spruce Street, Philadelphia, PA 19104, U.S.A.
[2] Applied Mathematics Research Center, Delaware State University, Dover, DE 19901, U.S.A.
{Cuiping.Zhang, Predrag.Bakic, Andrew.Maidment}@uphs.upenn.edu, Shugaoxia@gmail.com, Fliu@desu.edu

Abstract. Analysis of the breast surface deformation during mammographic compression will provide insight into breast tissue elastic properties. Our long term goal is to accurately estimate physical properties of breast tissue for the purpose of realistic deformation simulation. As a first step, we analyzed the acquisition accuracy of the reconstructed breast phantom surface using a non-contact laser scanner. The effect of the acquisition angle and the presence of the transparent compression plate covering the phantom were considered. Comparing 48 phantom surfaces, each reconstructed from 4 scanner images acquired at different positions, we observed an average acquisition error of 1.94 mm for images without the compression plate; the average acquisition error for images with the compression plate was 3.26 mm. Performance of two observers showed little variation.

Keywords: mammographic compression analysis, surface reconstruction, acquisition accuracy.

1 Introduction

This paper describes work in progress performed as part of our research on developing a framework for accurate estimation of breast tissue elastic properties. Physical compression of the breast during mammography causes deformation of the breast surface. Knowledge of breast tissue elastic properties would enable us to improve our existing 3D software breast tissue model [1] with realistic breast deformation simulation and would help in mammographic and tomographic image registration.

We plan to estimate breast elastic properties by analyzing the breast surface deformation and force distribution using a non-contact laser scanner. Non-contact scanners have been used in breast imaging for planning breast reconstructive surgery [2, 3]. They provide a noninvasive method to acquire accurate 3D measurements of the pre

E.A. Krupinski (Ed.): IWDM 2008, LNCS 5116, pp. 585–592, 2008.
© Springer-Verlag Berlin Heidelberg 2008

and post compression breast surface, making it possible to analyze breast surface deformation without the use of ionizing radiation. This is necessary to allow repeated measurements to be made.

Accurate acquisition of breast volume and surface data during mammographic breast compression is the first step toward analyzing breast deformation. This preliminary phantom study has been designed to validate accuracy of 3D breast surface acquisition from images acquired using a non-contact scanner. Our goal was to assess the effect of acquisition angle and the presence of a compression plate on the accuracy of the breast surface reconstruction.

2 Methods

2.1 Materials

A 5-cm thick non-deformable mammography quality control phantom (011A, CIRS, Norfolk, VA) was used in our preliminary study of the breast surface acquisition accuracy. We used a non-contact laser scanner (Vivid 910, Konica Minolta, Ramsey, NJ) to image the phantom. The scanner consists of a laser and a CCD video camera. A laser line is swept across the field of view using a rotating mirror that is controlled by a precise galvanometer. The scanned line is recorded by the CCD camera. The depth information of the scene is computed based on the position of scan line from the video sequence. Failure to capture a good image of the reflected laser line in the scene will result in surface data of poor quality. A polarized filter was mounted to the CCD camera in order to reduce the influence of specular reflection. The scanner image generated by the 3D scanner includes a point cloud, a polygonal-mesh and a 24-bit color image captured by the CCD camera.

2.2 Reconstruction of the Breast Phantom Surface from Laser Scanner Images

2.2.1 Camera-Phantom Positioning

The scanner is capable of generating 3D depth data for the phantom surface that is visible to the scanner. Generation of a complete phantom surface requires the registration and merging of several scanner images acquired at various camera-phantom positions. Fig. 1(a) illustrates the camera-phantom positioning by the azimuth, α, and elevation, ε, angles. The z-axis corresponds to the compression direction of the mammographic view, and the x-axis corresponds to the chest wall - nipple direction. In a clinical setting, the presence of the x-ray tube and gantry precludes the use of imaging directly from the top ($\varepsilon = 90^\circ$) or the front ($\alpha = 90^\circ$) of the breast. Therefore we acquired scanner images for 20 pairs of (α, ε) angles, where $\alpha \in \{0^\circ, 45^\circ, 135^\circ, 180^\circ\}$ and $\varepsilon \in \{0^\circ, 15^\circ, 30^\circ, 45^\circ, 60^\circ\}$.

Images of the non-deformable phantom were acquired with the phantom top covered by a transparent Lucite compression plate, corresponding to the clinical setting. To assess the effect of the compression plate, we also acquired phantom images at the same camera positions without the compression plate. The visible phantom area was manually segmented from scanner images. Fig. 1(b) shows a color image of the phantom positioning with the compression plate. Self-adhesive stickers of various colors

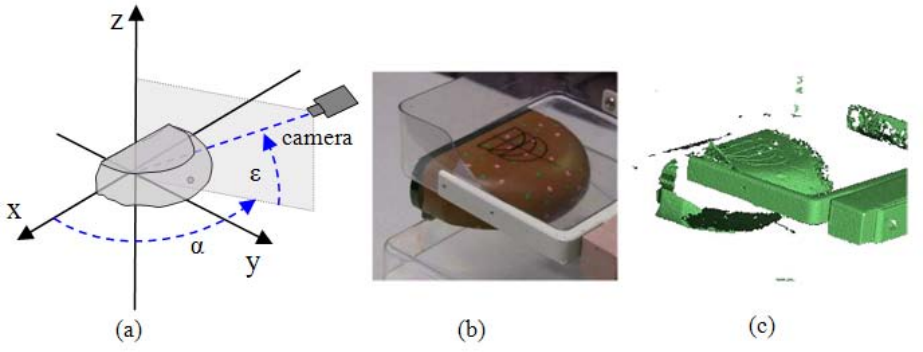

Fig. 1. Illustration of camera positioning. (a) Camera positions are labeled by azimuth α and elevation angles ε. (b) $\alpha = 45^{\circ}$, $\varepsilon = 30^{\circ}$ with the compression plate. (c) A 3D scanner image.

were used as fiducial points for registration purposes. Fig. 1(c) shows the corresponding 3D scanner image.

2.2.2 Registration and Merging of Scanner Images

Each scanner image, acquired at a specific camera-phantom position, includes the 3D depth data of the visible part of the phantom. Due to the presence of noise and background structures (as can be seen in Fig.1(c)), the original scanner images need to be processed to remove any non-phantom data. Images acquired from different positions are then registered and merged to a complete phantom surface using the software provided with the scanner. Pairs of scanner images (i.e., clouds of points) are registered using the Iterative Closest Point (ICP) algorithm [4], widely adopted to reconstruct 3D surfaces from different scans. Typically five or more feature points visible on both scans are manually labeled to initialize the registration and merge the surfaces. The merged 3D surface will cover most of the phantom area, except for the bottom side. To study the observer variation due to the manual data processing and feature point selection, two experienced observers performed the registration independently.

The final reconstructed surface is obtained by downsampling the number of vertices approximately 10-fold. This has the effect of smoothing the reconstructed surface.

2.3 Generation of the Phantom Ground Truth from CT Images

The reconstructed surfaces were compared to ground truth estimated from segmented CT images of the phantom. The CT images were acquired with a spatial resolution of 485 μm in-plane and 300 μm in the z-direction. The CT phantom data were segmented using a global optimal threshold [5], followed by morphological opening and closing to reduce the roughness of the phantom surface (Fig. 2 (a)).

2.4 Evaluation of the Reconstructed Phantom Surfaces

The reconstructed phantom surfaces and the ground truth estimate were downsampled to $(1.5\ \text{mm})^3$ resolution before comparison. A reconstructed 3D surface was aligned to the ground truth using a rigid transformation (3 displacements and 3 rotation

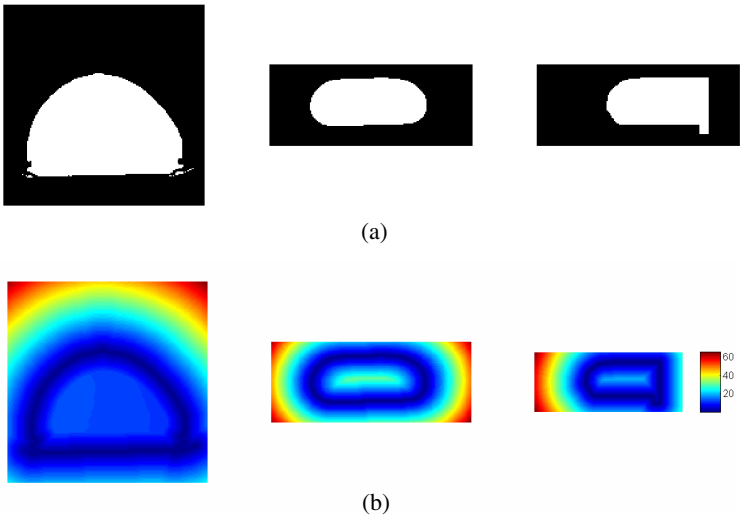

Fig. 2. (a) Orthogonal slices through the CT phantom data used as ground truth for surface evaluation. (b) Orthogonal slices of the distance map.

angles) that minimizes the mean squared error (MSE) between the phantom surface and the ground truth. We used the term "acquisition error" to refer to this error as it is largely attributed to different factors in the imaging process of the laser scanner. The optimal rigid transformation was computed using the Marquardt-Levenberg algorithm [6]. Due to the lack of 1-to-1 point correspondence between surfaces, the average distance between the two surfaces was computed using a distance map that was generated by a distance transformation [7] applied to the ground truth surface. Fig. 2 (b) shows orthogonal slices through the distance map corresponding to the ground truth from Fig.2 (a).

3 Results

3.1 Grouping and Selection of Individual Camera-Phantom Positions

Reconstruction of the whole 3D breast phantom requires the merging of several scanner images acquired at different camera-phantom positions. To minimize the total imaging time and the algorithm complexity, a small number of scanner images are desired. Previously we reconstructed a complete surface using 3 scanner images with two corresponding to each side view and one top view (along z-axis in Fig.3(a)) [8]. In a clinical setting, it is difficult to obtain a top view due to the presence of the mammography gantry and the x-ray tube. Therefore we used two images from each side with large elevation angles (close to the z-axis) instead of one top view image. Specifically, we divided all camera-phantom positions into 4 different groups and a complete phantom surface is merged by selecting one scanner image from each group. Fig. 3(a) illustrates the 4 groups on the x-z plane (i.e., chest wall plane). Table 1 shows the 4 groups in bold blocks.

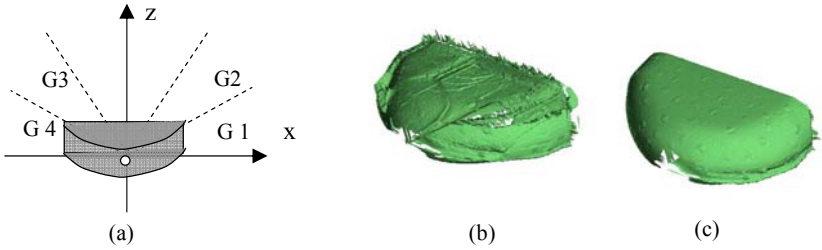

Fig. 3. (a) Illustration of 4 different viewing groups on the chest wall plane. Examples of reconstructed phantom surfaces: (b) with and (c) without (right) the compression plate.

Reliable registration of two scanner images requires the identification of several feature points visible in both images. As a result we analyzed only surfaces reconstructed using the scanner images indicated in Table 1. Combining one scanner image from each of the 4 groups (inside the bold rectangles) in Table 1, results in 24 different combinations to generate a reconstructed surface. Fig. 3(b) and 3(c) show examples of reconstructed surfaces with and without the compression plate.

Table 1. Scanner images used for reconstruction of 12 phantom surfaces

elevation **ε** azimuth **α**	0°	15°	30°	45°	60°
0°	**G1**	**G1**		**G2**	G2
45°					
135°		**G4**			
180°	G4	G4		G3	G3

3.2 Effects of Observer Variation on the Reconstructed Phantom Surfaces

The registration and merging of several scanner images into a complete phantom surface involves manual background removal and manual feature point selection. Two observers independently performed the phantom surface reconstruction with the 24 different combinations (from Table 1) for the phantom scanner images taken with and without the upper compression plate. As a result, 96 surfaces were generated. Table 2 compares the average values and the standard deviations of the acquisition errors. The error associated with the measure of the phantom surface for two observers is significantly different ($p<0.003$) without the compression plate. To reduce the observer variation and the error introduced by the compression paddle, we plan to develop an automated method for surface reconstruction.

Table 2. The average values and the standard deviation of the acquisition errors

Average acquisition error (mm)	with compression plate		without compression plate	
	observer 1	observer 2	observer 1	observer 2
average	3.33	3.19	1.92	1.95
stdev	0.41	0.29	0.15	0.14

3.3 Effects of the Compression Plate on the Reconstructed Surface

With the presence of the compression plate, the visibility of scanned surfaces was reduced due to refraction. Reconstructed surfaces have average acquisition errors of 3.26 mm and 1.94 mm, for images with and without the compression plate (Table 2). These average acquisition errors correspond to 2.17 and 1.29 voxels. Therefore, the presence of the compression plate increased the error by approximately one voxel. Fig. 4 shows

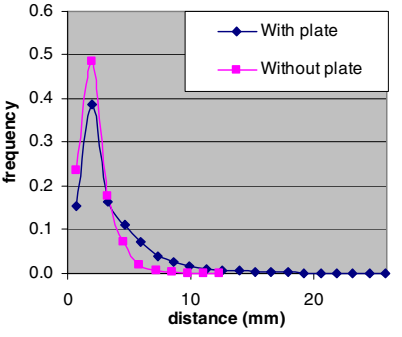

Fig. 4. Histograms of distances between the reconstructed and ground truth surfaces

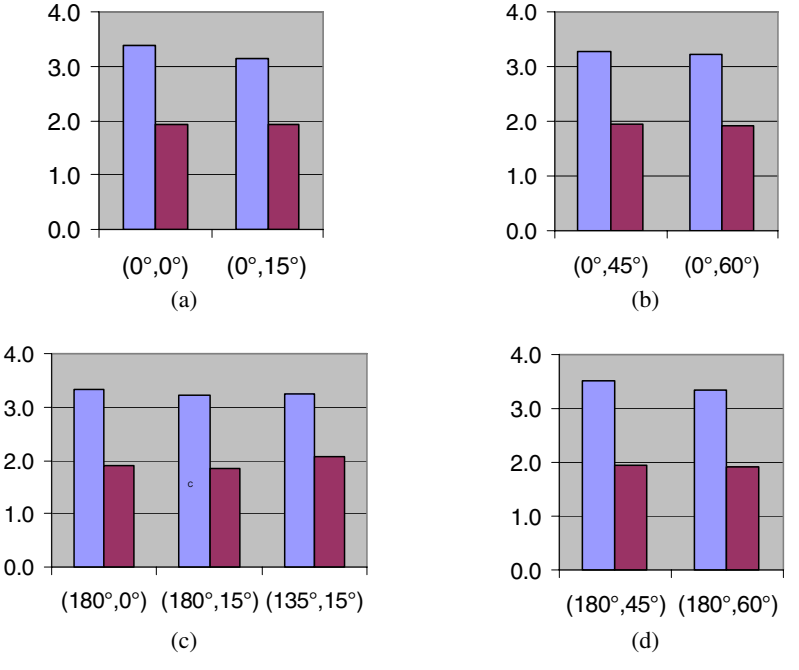

Fig. 5. Average acquisition errors (in mm) for reconstructed surfaces containing the scanner image acquired at position (α, ε), denoted as the azimuth and elevation angle pair. Subfigures (a) to (d) correspond to groups G1 to G4. Light (or dark) gray shows the results with (without) the compression plate.

the distribution of distances between the reconstructed and ground truth surfaces. For reconstruction with the compression plate, 54% of the distances are smaller than 3 mm (corresponding to two voxels). Without the plate, 72% of the distances are smaller than 3 mm.

3.4 Effect of Different Acquisition Angles on the Surface Accuracy

To assess the effects of azimuth and elevation angles on reconstruction accuracy, we compared the average acquisition errors for a selection of different scanner images as indicated in Table 1. As expected, errors for the surfaces with the compression plate (light gray) were consistently larger than without the plate (dark gray). Overall, the average difference between various acquisition angles belonging to the same group was relatively small (difference = 0.14 and 0.05 mm, with and without the compression plate, respectively). We also noticed that a larger elevation angle, $\varepsilon = 60°$ has slightly better performance compared to $\varepsilon = 45°$ (see Fig. 5(b) and Fig. 5(d)), as the top of the phantom is imaged under a smaller incident angle.

4 Discussions and Conclusions

In this preliminary experiment with a non-deformable phantom, we identified 4 groups of camera-phantom positions needed for an accurate surface reconstruction using a non-contact laser scanner. We analyzed the effect of the upper compression plate and the acquisition angle on the accuracy of the reconstructed breast phantom surface. We also evaluated the performance of different observers; the results show little observer variation. We are working on automatic feature point selection to reduce observer variation and improve the accuracy and repeatability of the results.

Our long term goal is to accurately estimate physical properties of breast tissue for the purpose of realistic deformation simulation. Analysis of reconstructed scanner images offers the possibility to estimate breast deformations corresponding to different stages of mammographic compression. Based on the estimated deformations and force measurements it is possible to calculate underlying material properties, with an assumption of uniform homogenous breast composition. More realistic assumptions are possible with the use of volumetric data, acquired with breast MRI [9] or tomosynthesis. However, non-contact optical scanning has the advantage of allowing repeated, non-invasive imaging of the same breast.

We observed an average acquisition error of 3.26 mm in reconstructing the shape of a non-deformable breast phantom; this error corresponds to an uncertainty of 7% in estimating the phantom thickness (t=5 cm). From the dependence of elasticity modulus on variations in compression force and breast thickness, this introduces 10% uncertainty in the estimation assuming we have accurate force measurement.

References

1. Zhang, C., Bakic, P.R., Maidment, A.D.A.: Development of an Anthropomorphic Breast Software Phantom Based on Region Growing Algorithm. In: SPIE Medical Imaging 2008: Visualization, Image-guided Procedures and Modeling, San Diego, vol. 6918 (2008)

2. Rodriguez-Larena, J., Canal, F.: Development of a 3D Digitizer for Breast Surgery Procedures. In: IS&T/SPIE Conference on Three-Dimensional Image Capture and Applications, San Jose, CA, pp. 226–233 (1999)
3. Tepper, O.M., Small, K., Rudolph, L., Choi, M., Karp, N.: Virtual 3-dimensional Modeling as a Valuable Adjunct to Aesthetic and Reconstructive Breast Surgery. American Journal of Surgery 192, 548–551 (2006)
4. Besl, P.J., McKay, N.D.: A Method for Registration of 3-d Shapes. IEEE Trans. Pat. Anal. and Mach. Intel. 14, 239–256 (1992)
5. Otsu, N.: A Threshold Selection Method from Gray-Level Histograms. IEEE Trans. Systems, Man and Cybernetics, 62–66 (1979)
6. Press, W.H., Teukolsky, S.A., Vetterling, W.T.: Numerical Recipes in C: The Art of Scientific Computing. Cambridge University Press, Cambridge (1992)
7. Friedman, J.H., Bentley, J.L., Finkel, R.A.: An Algorithm for Finding Best Matches in Logarithmic Expected Time. ACM Trans. Mathematics Software, 209–226 (1997)
8. Cao, J., Jackson, K., Liu, F., Pokrajac, D., Shi, X., Su, Z., Xia, S., Zhang, C., Bakic, P.: Analysis of 3D Breast Phantom Surface Deformation. In: Program of the 2nd Northeast Regional IDeA Meeting, Univ. of Vermont, Burlington, VT, p. 34 (August 2007)
9. Plewes, D.B., Bishop, J., Samani, A., Sciarretta, J.: Visualization and Quantification of Breast Cancer Biomechanical Properties with Magnetic Resonance Elastography. Physics in Medicine and Biology, 1591–1610 (2000)